

Experimental investigation of closed built-up sections using four cold-formed steel open sections under axial and eccentric loading

Shaokuai Wang¹, Lingfeng Yin^{*2}, Gan Tang³, Zhanjie Li⁴

Abstract

The light gauge steel structure (i.e., cold-formed steel framing) has been widely used in low-rise buildings for its ease of construction and high strength to weight ratio. However, this structural system is limited in member strength and stiffness and inhibits the flexibility of openings for doors and windows and also its use in mid-rise buildings and beyond. Innovation in cold-formed steel moment framing systems is needed. This study proposes a closed built-up section using four cold-formed steel open sections with a high load-bearing capacity that enables the development of high-performance cold-formed steel moment framing systems for mid-rise buildings and beyond. The closed section by combining four open cold-formed steel sections using fasteners can effectively enhance the local and distortional buckling load capacity of the sections under axial loading. Combining with specially designed intersections gusset plate this built-up section offers more potential configurations of beam-column moment connections for cold-formed steel structures. First, a heuristic optimization was performed based on the local and distortional buckling strength using the finite strip method. Second, a test program was developed to investigate the load-bearing capacity of this optimized closed section under axial and eccentric loading. The axial and eccentric loading tests of the built-up closed section column revealed the failure modes of the section under different loading conditions, axial and eccentric in the major-axis and weak-axis, and their load-carrying capacities. The study paved the groundwork for exploring high-performance cold-formed steel moment framing systems with this strong closed built-up section.

1. Introduction

With the increase of population and the increasing scarcity of land resources, the light gauge steel structure applicable to the lower floors is far from meeting the requirements of development. Therefore, it is especially important to explore the mid-rise structural system applicable to cold-formed thin-walled steel materials.

K.F. Chung [1-5] of the Hong Kong Polytechnic University conducted a systematic study on the force performance of cold-formed steel members and structures connected by bolts, and found that cold-formed steel has better performance through bolted connections and can transfer loads effectively. Theoretical and experimental studies were conducted by I. Georgieva et al. [6, 7] on collocated columns. The experimental results showed that when the length and slenderness of the members were relatively large, the failure modes were exhibited as bending and torsional instabilities and were more sensitive to the overall initial defects. Local

buckling phenomena occurred when the load was very small. The distortional buckling occurred near the ultimate load of the specimen, and the final failure demonstrated a combined yielding with the distortional buckling of the flange. A. B. Sabbagh [8, 9] proposed a new type of cold-formed thin-walled steel column with closed section and connected to the beam by means of pierced plywood, and focused on the performance of the beam-column connection. The connections have good ductile behavior and stiffness, which overcome the characteristics of traditional cold-formed thin-walled steel frame connections with weak stiffness and poor seismic performance.

This paper designs a cold-formed steel moment framing system with new combined section beams and columns as the main load-bearing members for mid-rise buildings and beyond, and proposes a column section applicable to this system - closed built-up sections using four cold-formed steel open section, as shown in [Figure 1](#). The load carrying capacity of the column section was optimized using the

¹ Shaokuai Wang. MA student, School of Civil Engineering, Southeast University, Nanjing, China, 220211186@seu.edu.cn

² Lingfeng Yin. Professor, School of Civil Engineering, Southeast University, Nanjing, China, eking@seu.edu.cn, Corresponding author

³ Gan Tang. Associate professor, Nanjing University of Aeronautics and Astronautics, Nanjing, China, tanggan@sina.com

⁴ Zhanjie Li. Associate Professor, Department of Engineering, SUNY Polytechnic Institute, Utica, NY, USA, Zhanjie.li@sunypoly.edu

CUFSM [10]. The experimental investigation on the bearing capacity of the closed built-up column is carried out to investigate the failure mode and ultimate bearing capacity under axial and eccentric compression.

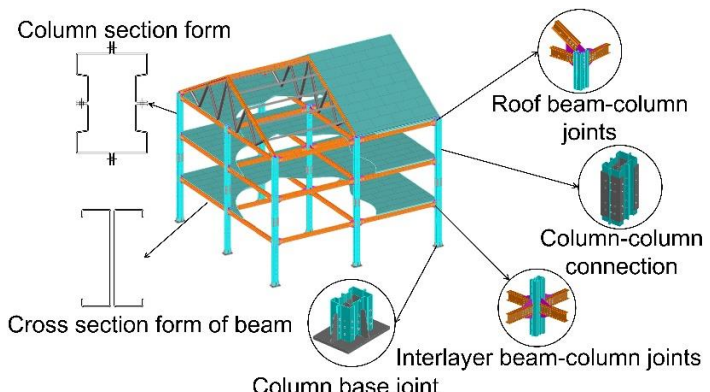


Figure 1: Cold-formed thin-walled section steel moment framing system

2. Optimization of closed built-up sections

A new closed section form (later referred to as "closed built-up sections") is proposed by combining the commonly used column sections in light gauge steel system and steel storage rack system, as shown in Figure 2.

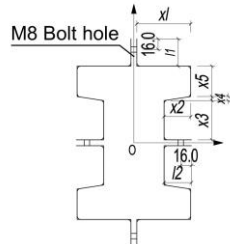


Figure 2: The Initial cross-section

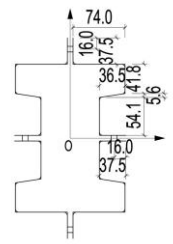


Figure 3: The final optimized cross-section

The initial cross-section was heuristically optimized using CUFSM, and the final optimized cross-section is shown in Figure 3, taking into account the installation and fabrication process requirements in the engineering practice. The cross-sectional properties and elastic flexural stress are shown in Table 1.

Table 1: Comparison of cross-sectional properties and elastic flexural stress

Section	Section properties					Axial pressure		Bending around strong axis		Bending around the weak axis	
	t mm	A_n mm ²	A mm ²	I_x cm ⁴	I_y cm ⁴	f_{ol} MPa	f_{od} MPa	f_{ol} MPa	f_{od} MPa	f_{ol} MPa	f_{od} MPa
Initial section	2.0	2208.0	2336.0	1948.28	667.19	910.8	648.6	1252.8	1250.7	1209.2	1681.9
Optimizing section	2.0	2208.0	2336.0	1517.86	643.42	1031.6	852.2	1257.9	1111.8	789.7	1173.6

The elastic local buckling stress is increased from 910.8 MPa to 1031.6 MPa, and the elastic distortion buckling stress is increased from 648.6 MPa to 852.2 MPa. As can be seen that these elastic buckling stresses are high (keep in mind that the yielding stress is 345MPa). The cross-section of the built-up column is a closed cross-section, and the resistance to distortion buckling is stronger. At the same time, because the cross-section has been rolled several times, the cross-section is complex with smaller plate width to thickness ratio, which improves the ability of the cross-section to resist local buckling. Therefore, the closed built-up section studied in this paper has superior performance in resisting local and distortional buckling.

Similar performance can be observed based on the elastic buckling analyses of the optimized closed built-up section under the strong and weak axes. Hence, the optimized closed built-up section is expected to have good performance in resisting local and distortional buckling under eccentric loading.

3. Experimental Program

3.1 Material properties

According to Metallic materials tensile test Part 1: room temperature test method GB/T 228.1-2010 [11] and Sampling Location and Specimen Preparation for Mechanical Properties Test of Steel and Steel Products GB/T2975-1998 [12], a one-way tensile test was conducted to measure the materiality of the components used in this test.

Figure 4 shows the failure of the specimens cut from the flat area, and Figure 5 shows the failure of the specimens cut from the corner area.



Figure 4: Specimens after tensile fracture cut from the flat plate



Figure 5: Specimens after failure cut from the corner area

Through the tensile tests of the flat plate area and the corner area the material properties can be obtained from the stress-

strain curves. The modulus of elasticity E is 2.037×10^5 MPa from specimens cut from both areas. In the flat plate the nominal yield strength is 341.05 MPa, and the ultimate strength is 421.58 MPa, while in the corner area the yield strength is 403.44 MPa, about 18% higher than that of the flat area, and the ultimate strength is 471.86 MPa, about 12% higher than that of the flat area.

3.2 Load carrying tests of closed built-up columns

3.2.1 Specimen dimensions

The test specimen is designed for the closed built-up column made of four cold-formed steel open sections with high-strength bolts. To meet the needs of beam-column connection in the framing, a connection plate is made of pierced steel plate, the thickness of which is initially proposed to be 6 mm. The material of the built-up column is Q345, the thickness of open sections is 2 mm, and the high-strength bolt is M8 with a spacing of 500 mm longitudinally. The distance of the bolts from the edge of the column in the transverse direction is 2 times the diameter of the bolts. At

3.2.2 Test setup

The axial and eccentric loading tests of the built-up closed section column was completed in the structural test

laboratory of Southeast University. The loading equipment used in the test was MTS 100t fatigue testing machine. The loading system is shown in Figure 7(a), and the measurement locations are shown in Figure 7(b).

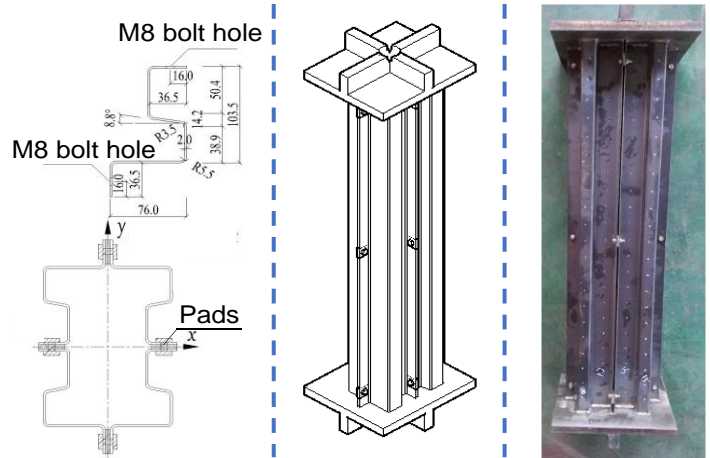
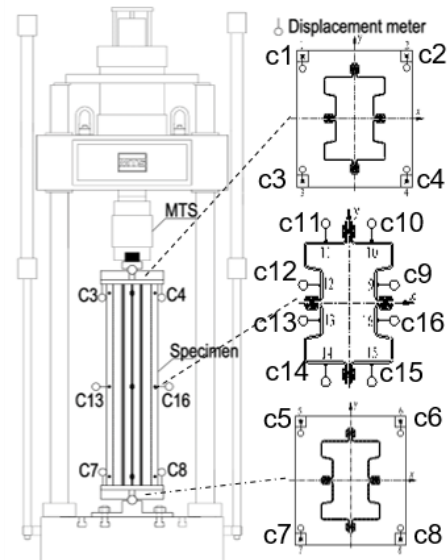


Figure 6: Specimen size, 3D schematic view, and tested specimen

laboratory of Southeast University. The loading equipment used in the test was MTS 100t fatigue testing machine. The loading system is shown in Figure 7(a), and the measurement locations are shown in Figure 7(b).



(a) Loading system



(b) Measurement locations

Figure 7: Test setup

In order to investigate the bearing capacity of the column, the test was set up to be under possibly axial loading and , uniaxial or biaxial eccentric loadings.

The closed built-up column is a biaxial symmetric section. As shown in Figure 8(a), point O is the geometric center of

the section, For eccentric loading, A is a loading point, and the location of the loading point can be determined by their coordinates x_1 and y_1 as shown. In addition, the angle can also be determined. For this study, due to the symmetry, loading points were selected to be only in 1-quadrant. α

takes 0° , 30° , 60° , 90° , and nine loading points are selected in the direction of these special angles, as shown in Figure 8(b). Thus, these 9 loading points correspond to ten specimens, and two axially compressed specimens are also tested, and the total number of test specimens is 10. The specific locations of the load points are listed in Table 2.



(a) Load point positioning parameters (b) Load Point Distribution
Figure 8: Load point positioning parameters and distribution map

Table 2: Sample table of numbers

Type of pressure	Specimen number	Theoretical load point location		
		$\alpha(^{\circ})$	$x_1(\text{mm})$	$y_1(\text{mm})$
Axial pressure	A-0-0(1)	0	0.0	0.0
	A-0-0(2)	0	0.0	0.0
Unidirectional eccentric	U-0-50	0	50.0	0.0
	U-0-100	0	100.0	0.0
	U-90-50	90	0.0	50.0
	U-90-100	90	0.0	100.0
Bi-directional eccentric	B-30-50	30	43.30	25.0
	B-30-100	30	86.60	50.0
	B-60-50	60	25.0	43.30
	B-60-100	60	50.0	86.60

* Numbering Rules: Type of pressure – α - Distance to point O

3.2.3 Initial geometric imperfections

Six of the ten members in this study were randomly selected for initial imperfection measurement, and the initial imperfections of these six specimens were used to reveal the initial imperfections of this batch of specimens. Cross-sectional properties are shown in Table 3. The initial imperfections of the specimens were measured using the method suggested in the literature [13], and the statistical

results of the maximum initial defect values measured for each specimen are shown in Table 4.

Table 3: Cross-sectional properties

Cross-section area (mm ²)	Strong axis inertia moment(m ⁴)	Weak axis inertia moment(m ⁴)
2058.536	1.41498×10^{-5}	6.01153×10^{-6}

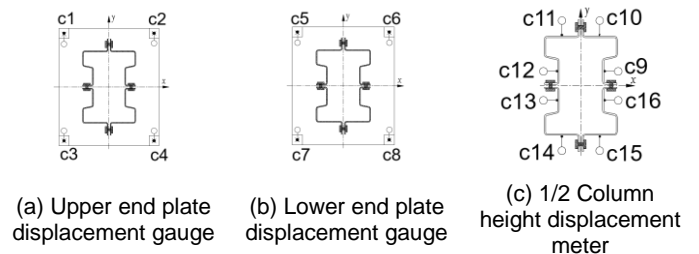
Table 4: Initial geometric imperfection measurement of each specimen

Specimen number	Geometric imperfection location	Measured Value (mm)	Specimen number	Geometric imperfection location	Measured value/mm
A-0-0(1)	Webs	1.021	U-90-50	Webs	1.333
	Edge of flange	0.699		Edge of flange	0.539
U-0-50	Webs	1.398	U-90-100	Webs	1.089
	Edge of flange	0.645		Edge of flange	0.808
U-0-100	Webs	0.977	B-30-50	Webs	1.069
	Edge of flange	0.716		Edge of flange	0.706

3.2.4 Sensor plan

Displacement measurement mainly includes axial compression displacement, lateral displacement and end rotation of the column. In order to accurately measure and record the deformation of the specimen during the test, a total of eight vertical displacement gauges were placed at the corner points on the end plates at both ends of the specimen, as shown in Figure 9(a) and (b). Eight lateral displacement gauges are placed at the 1/2 column height

section of the specimen (as shown in Figure 9(c)).



(a) Upper end plate displacement gauge (b) Lower end plate displacement gauge (c) 1/2 Column height displacement meter
Figure 9: Displacement gauge arrangement (top view)

4. Results and discussions



4.1 Axially compressed specimen

4.1.1 Load-axial displacement curve

Axially compressed specimens are 2 specimens with the same dimensions, and the specimens behaved as stub column without obvious cross-sectional buckling failure. However, it did form a plastic section at the 1/2 column height section of the specimen with minor-axis bending. The bolts behave well throughout the loading process without pulling off and obvious loosening, ensuring the integrity of the built-up section.

In the initial stage of loading, the axial displacement grew linearly with the load, and the stiffness of the specimen was basically unchanged at this time. Until the load was loaded near the ultimate load, the specimen entered the plastic stage with nonlinearity. The displacement increased rapidly to the peak. After crossing the peak, the load decreased rapidly until the specimen was failed. The test results are shown in Table 5.

Table 5: Test results

	A-0-0(1)	A-0-0(2)
Axially compressed specimen deformations after test unloading		
P_T (kN)	605.58	628.32
Failure mode	L+G	

*L for Local buckling and G for Global buckling

4.1.2 Load-lateral displacement curve

The load-lateral displacement curves of the axially compressed specimen are plotted in Figure 10.

Combined with the test phenomenon the axially compressed specimen showed almost no lateral displacement until

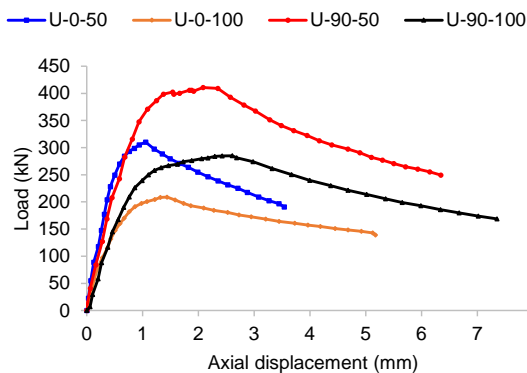


Figure 11: Load-axial displacement curves and failure of uniaxial eccentric specimens

loaded near the ultimate load. With the accumulated plasticity, the lateral bending of the column around the Y axis started to develop. The displacement curves of No. 9 and No. 16 almost overlapped, and No. 12 and No. 13 were also close, which means that section produced a symmetrical overall lateral displacement - no torsion. The displacement values of No. 9 and No. 16 are greater than those of No. 12 and No. 13, indicating that the deformation value of the inner side of the bending was greater than those of the tensile side of the bending.

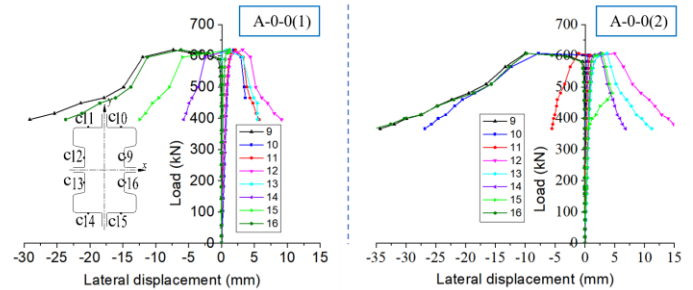


Figure 10: Load-lateral displacement curves of axially compressed specimen

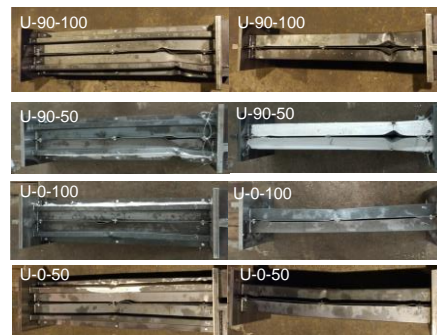
4.1.3 Ultimate bearing capacity

The ultimate bearing capacity can be obtained from the test for closed built-up column under axial compression. The failure as aforementioned occurred at the middle-height of the column with an inelastic local buckling followed by flexural buckling about the weak axis due to the localized plastic section of local buckling.

4.2 Uniaxial eccentric loaded specimen

4.2.1 Load-axial displacement curves

There are four specimens under uniaxial eccentric loading about the X-axis (U-90-50 and U-90-100) and the Y-axis (U-0-50 and U-0-100). The load-axial displacement curves of the uniaxial eccentric loading specimen are shown in Figure 11.



Uniaxial eccentric loaded specimen deformations after test unloading

The impact of the eccentricity can be observed from the load-displacement responses. The axial load carrying capacities showed significant reduction compared to the same eccentricity distance about minor axis compared to those of the major axis (i.e., U-90 vs. U-0 specimens). With the increase of the eccentricity (i.e., 50 vs. 100), the axial load carrying capacities also decreased significantly. Under the eccentricity about X axis (i.e., U-90 specimens), the failure demonstrated an inelastic local buckling at 1/2 column height while under the eccentricity about the Y-axis the inelastic local buckling failure were at a distance of about 25 cm from the bottom end. When 75% of the ultimate load was reached, the flanges near the bolts began to deform locally, and the flanges on both sides of the area about 25cm away from the top and bottom ends plate was pinched and separated respectively, and the plate underwent local buckling. When the ultimate load was reached, The column did not experience global buckling.

4.2.2 Load-lateral displacement curve

The load-lateral displacement curves of each uniaxial eccentrically loaded specimen are plotted in Figure 12. The displacement gauges arrangement were the same as that of the axially loaded specimen.

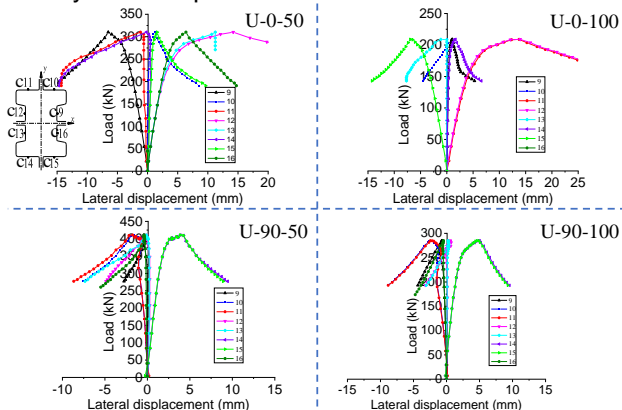
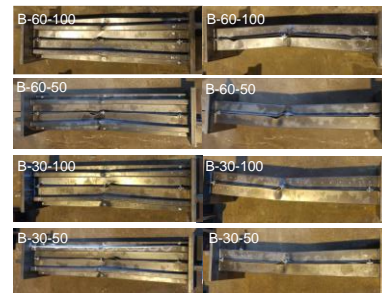
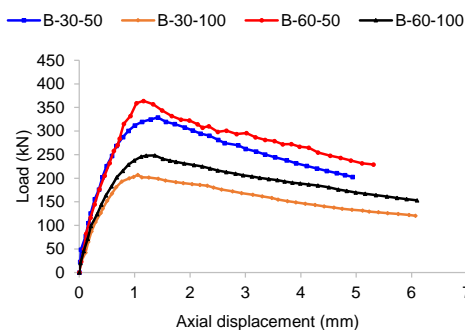


Figure 12: Load-lateral displacement curve of unidirectional eccentric compressed specimen

The displacement in the web of specimens U-0-50 and U-0-100 is positive on one side and negative on the other side,



Biaxial eccentric loaded specimen deformations after test unloading

Figure 13: Load-axial displacement curves and failure of biaxial eccentric loaded specimen

and the difference between the curves on magnitude is not large, indicating that the overall lateral bending of the specimen occurs with no torsion. Specimens U-0-50, U-0-100 flange deformation bent almost simultaneously from the initial stage of loading. Before peak, other than the 14 and 15 displacement gauges the displacement of the rest was small. Displacements of 14 and 15 were almost the same.

4.2.3 Ultimate bearing capacity

The ultimate bearing capacity and failure mode of the uniaxial eccentric loaded specimen are summarized in Table 6.

Table 6: Unidirectional eccentric compressive specimen test load capacity and failure mode

Specimen number	Failure mode	Failure location	Ultimate load P_T (kN)
U-0-50	G	1/2 column height	311.83
U-0-100	G	1/2 column height	210.23
U-90-50	L	25cm from the bottom end plate	411.67
U-90-100	L	25cm from the bottom end plate	286.54

*G for Global buckling; L for Local buckling

4.3 Biaxial eccentric loaded specimen

4.3.1 Load-axial displacement curves

Four specimens are subjected to eccentricities in two directions. All the specimens showed the failure was located near the 1/2 column height. Due to the biaxial bending effects, the failure modes of the specimens were different for those of uniaxial eccentric loaded specimen. The Load-axial displacement curves and failure of biaxial eccentric loaded specimen are shown in Figure 13.

When the eccentricity distance is the same, the eccentricity direction has an effect on the bearing capacity of the specimen. Combined with the specimens with uniaxial eccentricity in the previous section, it is found that the bearing capacity is increasing with the rotation of the eccentricity angle from the X axis to the Y axis, i.e. the larger the value of the eccentricity angle α (as in Figure 8(a)), the larger the bearing capacity of the specimen. The four specimens with biaxial eccentricity loading have global buckling in two directions, but the global buckling around the Y-axis was the main one, and the failure areas were located near 1/2 of the column height. For specimen B-60-100, when 80% of the ultimate load was reached, the flange of the specimen began to deform, and the flange gap began to close. When the ultimate load was reached, the open section plate on the compression side appeared bulging, with obvious local buckling. The specimen underwent lateral global buckling.

4.3.2 Load-lateral displacement curve

The load-lateral displacement curves of each biaxial eccentrically loaded specimen are shown in Figure 14.

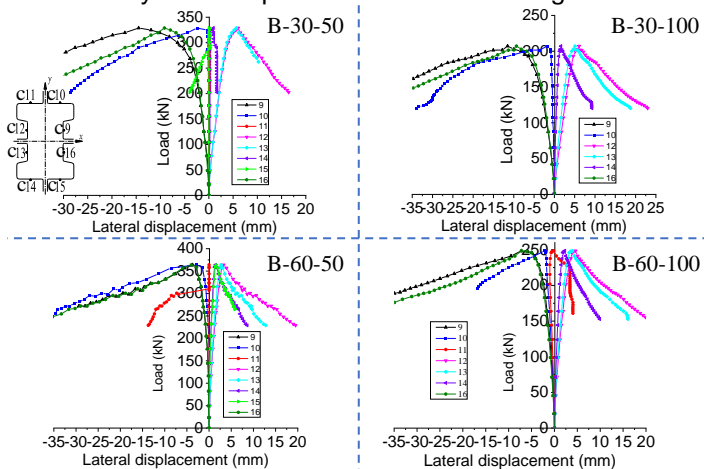


Figure 14: Load-lateral displacement curve of biaxial eccentric loaded specimen

The curves of load-lateral displacement of each specimen showed a consistent pattern, indicating that similar deformation occurred in the cross section here. The specimen underwent lateral bending in both directions, as shown by the fact that the displacement at 9 was greater than that at 10. The rotation about the Y axis was more obvious and the displacement was greater.

Unlike the uniaxial eccentrically loaded specimen, displacements at 9 and 10 in the quadrant where the load were located were greater than those at 16 and 11 indicating that the bending phenomenon occurring in this column side was greater than the other side. The specimen was twisted as well.

4.3.3 Ultimate bearing capacity

The axial load carrying capacity of the biaxially eccentrically-loaded specimen and failure mode are listed in Table 7.

Table 7: Bearing capacity and failure mode of biaxially eccentrically-loaded specimen test

Specimen number	Failure mode	Failure location	Ultimate load P_T (kN)
B-30-50	G	1/2 column height	330.58
B-30-50			
B-30-100	G	1/2 column height	217.18
B-30-100			
B-60-50	G	1/2 column height	363.99
B-60-50			
B-60-100	L+G	1/2 column height	249.05
B-60-100			

*G for Global buckling; L for local buckling

7. Conclusions

For the cold-formed thin-walled section steel built-up column, the mechanical properties of materials test, bearing capacity tests under axial and eccentric compression were carried out, and the failure of each specimen and related test data were obtained. Through the detailed analysis of the test phenomena and test results of each specimen, some conclusions can be drawn. The axially compressed specimen underwent an inelastic local buckling followed with flexural buckling about the weak axis. Under uniaxial eccentric loading, the failure modes showed different patterns under eccentricities in X and Y directions. The impact of the eccentricities were large in the X direction (i.e., eccentricity about Y axis). For the biaxial eccentric loading, the overall bending failure occurred, in which the bending amplitude around the weak axis was greater and more obvious with the phenomenon of local buckling in the central failure section. The deformation of the column piece in the load quadrant was greater. Meanwhile, the high-strength bolts connecting the open sections showed no pulling off and loosening or slipping.

8. Acknowledgments

This work was sponsored by the Natural Science Foundation of Jiangsu Province (BK20191268); and the Project of Central Government for Local Science and Technology Development of Tibetan Autonomous Region (XZ202201YD0032C).

References

- [1] Chung KF, Lau L. Experimental investigation on bolted moment connections among cold formed steel members. *Engineering Structures* 1999;21:898-911. [https://doi.org/10.1016/S0141-0296\(98\)00043-1](https://doi.org/10.1016/S0141-0296(98)00043-1).

- [2] Chung KF, Lawson RM. Structural performance of shear resisting connections between cold-formed steel sections using web cleats of cold-formed steel strip. *Engineering Structures* 2000;22:1350-66. [https://doi.org/10.1016/s0141-0296\(99\)00083-8](https://doi.org/10.1016/s0141-0296(99)00083-8).
- [3] Chung K, Wong M. Experimental investigation of cold-formed steel beam-column sub-frames: enhanced performance. *Structural Engineering, Mechanics and Computation: Elsevier*; 2001. p. 1515-22.
- [4] Wong MF, Chung KF. Structural behaviour of bolted moment connections in cold-formed steel beam-column sub-frames. *Journal of Constructional Steel Research* 2002;58:253-74. [https://doi.org/10.1016/s0143-974x\(01\)00044-x](https://doi.org/10.1016/s0143-974x(01)00044-x).
- [5] Yu WK, Chung KF, Wong MF. Analysis of bolted moment connections in cold-formed steel beam-column sub-frames. *Journal of Constructional Steel Research* 2005;61:1332-52. <https://doi.org/10.1016/j.jcsr.2005.03.001>.
- [6] Georgieva I, Schueremans L, Pyl L, Vandewalle L. Experimental investigation of built-up double-Z members in bending and compression. *Thin-Walled Structures* 2012;53:48-57. <https://doi.org/10.1016/j.tws.2011.12.017>.
- [7] Georgieva I, Schueremans L, Vandewalle L, Pyl L. Design of Built-Up Cold-Formed Steel Columns According to the Direct Strength Method. *Procedia Engineering* 2012;40:119-24. <https://doi.org/10.1016/j.proeng.2012.07.066>.
- [8] Sabbagh AB, Petkovski M, Pilakoutas K, Mirghaderi R. Ductile moment-resisting frames using cold-formed steel sections: An analytical investigation. *Journal of Constructional Steel Research* 2011;67:634-46. <https://doi.org/10.1016/j.jcsr.2010.11.016>.
- [9] Sabbagh AB, Petkovski M, Pilakoutas K, Mirghaderi R. Cyclic behaviour of bolted cold-formed steel moment connections: FE modelling including slip. *Journal of Constructional Steel Research* 2013;80:100-8. <https://doi.org/10.1016/j.jcsr.2012.09.010>.
- [10] Li Z, Schafer BW. Buckling analysis of cold-formed steel members with general boundary conditions using CUFSM conventional and constrained finite strip methods. 2010.
- [11] GB/T 228.1-2010. Metallic materials tensile testing at ambient temperature. China Standard Press; Beijing, China; 2010 [in Chinese].
- [12] GB/T 2975-1998. Steel and Steel Products-Location and Preparation of Samples and Test Pieces for Mechanical Testing. China Standard Press; Beijing, China 2018 [in Chinese]. GB.
- [13] Young B, Liu YH. Experimental investigation of cold-formed stainless steel columns. *Journal of Structural Engineering-Asce* 2003;129:169-76. [https://doi.org/10.1061/\(ASCE\)0733-9445\(2003\)129:2\(169\)](https://doi.org/10.1061/(ASCE)0733-9445(2003)129:2(169)).